Vietnam Journal of Science and Technology ***64***(3) (2026) 576–593
DOI: https://doi.org/10.15625/2525-2518/21413

Investigation and optimization for enhanced machining features of heat-treated SKD61 steel as processed by powder-mixed electro-discharge machining in finishing regime

Van-Tao Le[1,*], Thi Hong Minh Nguyen[2], Tien Dung Hoang[3]

[1]*ATC, Le Quy Don Technical University, 236 Hoang Quoc Viet, Nghia Do Ward, Ha Noi, Viet Nam*
[2]*SME, Hanoi University of Science and Technology, 1 Dai Co Viet, Bach Mai Ward, Ha Noi, Viet Nam*
[3]*SMAE, Hanoi University of Industry, 298 Cau Dien, Tay Tuu Ward, Ha Noi, Viet Nam*

[*]Email: *levantao@lqdtu.edu.vn*

Received: 27 August 2024; Accepted for publication: 3 March 2025

Abstract. Machinability investigation of SKD61 steel in heat-treated state as machined by electro-discharge machining (EDM) in finishing regime with adding tungsten compound powder is very restrictive. Hence, the machinability of this material state, comprising rate of material removal (RMR), rate of electrode wear (REW), and surface roughness (R_a), was explored under the influence of control parameters {including peak-current (I_p), pulse-on time (T_{on}), and powder amount (A_p)}. In addition, finding the optimal domain of control parameters is meaningful in improving the RMR, R_a, and reducing REW. With this goal, the predictive models for RMR, R_a, and REW were instituted and evaluated to confirm these models' adequacy and accuracy by the analysis of variance (ANOVA). Eventually, desirable approach (DA) and technique for order of preference by similarity to ideal solution (TOPSIS) were executed for the multi-criteria optimization. The results revealed that I_p proves the most robust influence on RMR, REW, and R_a. However, the sequent influences are A_p and T_{on} for REW, while the reverse is for R_a. The value of RMR by DA is increased by 8.67 % versus TOPSIS. Meanwhile, the TOPSIS contributes the best optimum solution for REW and R_a, corresponding to a drop of 10 % and 0.5 % versus DA. In addition, surface features (defects, chemical composition distribution, TRL, surface topography, and crack acreage percentage (CAP)) at optimal parameters of the two algorithms were also considered.

Keywords: PMEDM, RMR, REW, surface attributes, multi-criteria optimization.

Classification numbers: 5.1.1, 5.7.1, 2.5.3.

1. INTRODUCTION

SKD61 tool steel is widely applied in manufacturing due to its excellent high-temperature resistance, corrosion resistance, oxidation resistance, and toughness, especially after heat treatment [1]. It is commonly used for producing molds such as hot stamping, plastic, and blow molds [2]. Although heat-treated SKD61 is difficult to machine by conventional methods, it is suitable for electro-discharge machining (EDM) [3]. However, EDM has low productivity and

causes surface defects [4]. Recently, powder-mixed EDM (PMEDM), which introduces conductive particles into the dielectric fluid, has been developed to enhance machining efficiency and surface quality [5].

PMEDM studies on SKD61 steel have mainly focused on the non-heat-treated state. For instance, EDM with surfactant and Al powder additions was investigated to evaluate the effects of discharge current, pulse-on time, and powder concentration on thickness of recast layer (TRL) and surface roughness (SR) [6]. The results confirmed significant effects of these parameters on TRL and SR improvement. Other studies using Cr and Al powders in different dielectric fluids reported that pulse-on time, peak current, dielectric type, powder ratio, and particle size influenced material removal rate (MRR), SR, and electrode wear rate (EWR) [7]. Moreover, Mo powder-assisted EDM with a rotating electrode was found to enhance surface modification, carbide formation, and hardness [8]. The effects of electrode area and electrical parameters during EDM with Si powder were also examined, showing that an appropriate powder concentration is essential for improving SR [9]. Recently, tungsten powder-assisted EDM was reported to modify surface chemistry, enhance hardness, and induce new phases [10]. However, the heat-treated state of SKD61 steel remains insufficiently investigated despite its extensive industrial applications.

Improving machining efficiency and product quality requires effective process parameter optimization. Various multi-objective optimization methods, such as PSO, GA, AMGA, NSGA-II, BFO, Taguchi, and GRA, have been applied. However, most of these techniques only provide Pareto solutions and are limited in identifying a global optimum [11]. Therefore, TOPSIS and desirability approach (DA) are effective methods for solving multi-criteria problems and obtaining a single optimal solution.

The combination of EDM with tungsten compound powder mixed in a dielectric fluid for machining heat-treated SKD61 steel is highly significant. Tungsten possesses excellent physical, chemical, and mechanical properties, including a high melting point (~3422 °C), low thermal deformation, high thermal conductivity, thermal strength, corrosion resistance, oxidation resistance, and hardness, making it suitable for surface modification applications. However, research on heat-treated SKD61 steel processed by tungsten powder-assisted EDM remains limited.

Hence, exploring the machinability of the heat-treated SKD61 steel by EDM machining with tungsten compound powder at finishing regime is necessary, and has significance in production and research. To solve this problem, a relationship between the various machining parameters {powder amount (A_p), pulse-on time (T_{on}), and peak-current (I_p)} and the machining features {RMR, REW, and SR} was instituted by math models. Subsequently, the influences of machining parameters on the machining features (including RMR, REW, and SR) were investigated. Finally, to improve the machining features, the optimum problem of simultaneously finding the minimum REW and R_a, and the maximum RMR was implemented by the DA and TOPSIS to choose a reasonable solution for each machining feature. Besides, the surface features (defects, chemical composition distribution, TRL, surface topography, and crack acreage percentage (CAP)) at optimal parameters of the two algorithms were also considered. These help to have more knowledge and understanding of the finishing regime of EDM process engaging tungsten compound powder.

2. MATERIALS AND METHODS

2.1. Materials and processes

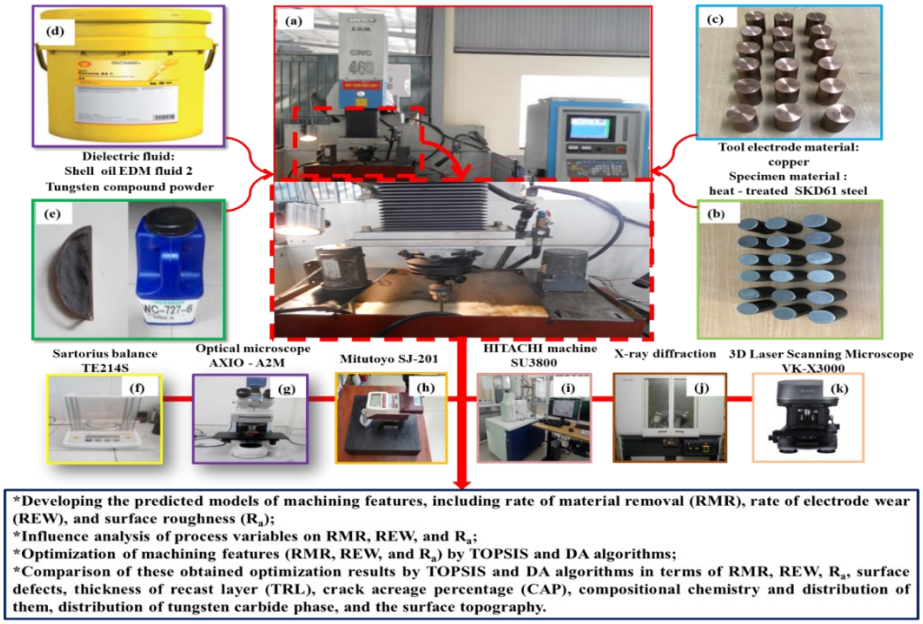

Figure 1. Empirical diagram of the study.

Figure 1b shows the SKD61 steel specimens with dimensions of 45 × 19 mm (height × diameter). The initial composition consisted of C (0.38 %), Mn (0.4 %), V (1 %), Si (1 %), Mo (1.25 %), Cr (5 %), and Fe as the balance (wt.%). After heat treatment, the specimens reached a hardness of 50 ± 2 HRC. The treated material contained Mn (0.54 %), C (21.16 %), Si (0.53 %), O (19.4 %), V (0.66 %), Mo (3.18 %), Cr (3.28 %), and Fe as the balance (wt.%). The experiments were conducted using an Aristech CNC-460 EDM machine with a 99 % Cu electrode under reverse polarity conditions (Figures 1a and 1c). Tungsten compound powder with a particle size below 31 µm, containing C (5.56 %), W (82.5 %), Co (11.9 %), Fe (0.02 %), and other elements (0.02 %) (wt.%), was uniformly mixed into Shell EDM 2 dielectric fluid (Figures 1d and 1e).

2.2. Empirical procedure

The selection of processing variables was based on previous studies and the available settings of the EDM machine. This study evaluated the effects of control parameters on the machinability of the heat-treated material, including MRR, Ra, and TWR, during fine-finishing operations. Since pulse-on time (T_{on}) and peak current (I_p) significantly affect machining performance [12], they were chosen as variables, while voltage (120 V) and pulse-off time (40 µs) were kept constant. The powder concentration (A_p) was determined through preliminary experiments considering the electrical and thermal properties of the powder. Therefore, T_{on}, I_p, and A_p were selected as input factors for the DOE. A Box–Behnken design based on RSM was applied to reduce the number of experiments and costs while maintaining model reliability. The selected parameter levels were determined according to EDM machine limitations, powder properties, and previous studies [13], as shown in Table 1.

Table 1. Matrix of process variables and output responses.

No.	Machining parameter			Measured response (avg.)		
	T_{on} (µs)	I_p (A)	A_p (g/L)	REW (g/min)	RMR (g/min)	R_a (µm)
1	80	3	20	0.000783	0.00629	2.4
2	20	2	10	0.000363	0.00364	2.01
3	50	2	0	0.000612	0.00348	2.28
4	80	2	10	0.000673	0.00438	2.17
5	50	4	0	0.001995	0.00688	3.12
6	50	3	10	0.000639	0.00482	2.38
7	80	4	10	0.001932	0.00791	3.16
8	50	2	20	0.000490	0.00446	1.98
9	20	4	10	0.001055	0.00611	2.52
10	20	3	20	0.000649	0.00443	2.09
11	20	3	0	0.000876	0.00404	2.48
12	50	3	10	0.000662	0.00493	2.41
13	80	3	0	0.001478	0.00532	2.94
14	50	3	10	0.000663	0.00465	2.39
15	50	4	20	0.001063	0.00810	2.75

2.3. Measurement of output variables

The surface roughness (R_a) was measured using a Mitutoyo tester (Figure 1h), initially set up with a cutoff length of 0.8 mm and a track length of 4 mm. The mean values of the three distinct measurement regions on the sample's machined surface represented the surface roughness value for each technological mode. Subsequently, RMR and REW were computed by Eqs. (1) and (2). The electrode and specimen weights were measured using a Sartorius electronic balance (Figure 1f). The machining time in Eqs. (1) and (2) is the time required to change the height of the sample from 45 mm down to 44.3 mm. The results of RMR, REW, and R_a are presented in Table 1. A HITACHI SU3800 machine (Figure 1i) was used to determine the content, distribution, and chemical composition of elements on the surface using energy dispersive X-ray spectroscopy (EDS), in which the element content is the average value of three different areas. The recast layer of the specimens was obtained by an optical microscope (AXIO - A2M as in Figure 1g) as it went through various processing phases [14], and the recast layer was computed according to Eq. (3). The crack acreage percentage (CAP) on the surface of the specimen was obtained as it underwent various processing stages [14], and CAP was computed according to Eq. (4). The topography of the machined surfaces was observed and examined using a 3D laser scanning microscope (VK-X3000, Keyence Corporation), and multi-file analysis software for analysis in the following section.

$$RMR\left(\frac{g}{min}\right) = \frac{Workpieceweightbeforemachining - Workpieceweightaftermachining}{Machiningtime} \quad (1)$$

$$REW\left(\frac{g}{min}\right) = \frac{Electrodeweightbeforemachining - Electrodeweightaftermachining}{Machiningtime} \quad (2)$$

$$\mathrm{TRL}(\mu\mathrm{m}) = \frac{\sum_{i=1}^{3} \frac{A_{\mathrm{recastlayer(i)}}}{L_{\mathrm{recastlayer(i)}}}}{3} \quad (3)$$

$$\mathrm{CAP}(\%) = \frac{\sum_{i=1}^{3} \frac{\sum A_{micro-crack(i)}}{A_{\mathrm{micrograph\ of\ SEM}(i)}}}{3} * 100\% \quad (4)$$

3. RESULTS AND DISCUSSION

3.1. Main influence analysis and development of mathematical models for machining features

Figures 2a–c present the main effects of machining parameters on the process responses, confirming that T_{on}, I_p, and A_p significantly affect all machining characteristics. As shown in Fig. 2a, increasing T_{on}, I_p, and A_p enhances RMR throughout the investigated range. This is attributed to the higher thermal energy generated at elevated T_{on} and I_p, which promotes material melting and removal from the workpiece surface [16]. In addition, powder particles suspended in the dielectric reduce fluid viscosity, facilitating the ejection of molten materials and improving RMR [17]. Figure 2b illustrates that REW increases with increasing T_{on} and I_p, whereas a higher A_p reduces electrode wear. The proper combination of these parameters generates favorable discharge conditions, increasing powder concentration in subsequent discharges and improving heat distribution [18]. Consequently, the thermal load transferred to the electrode decreases, reducing melting and evaporation of electrode material [13]. Figure 2c indicates that R_a increases with higher T_{on} and I_p but decreases as A_p rises from 0 to 20 g/L. This improvement is attributed to the suitable interaction among T_{on}, I_p, and A_p, which enhances discharge stability and uniformity through the formation of a stable discharge channel with a higher powder concentration [18].

The predictive models of RMR, REW, and R_a were set up and correspond to Eqs. (5(7).

$$RMR = 0.00664 - 0.000008T_{on} - 0.003133I_p - 0.000042A_p + 0.000710\ I_p^2 + 0.000002A_p^2 - 0.0000000002778T_{on}^2 + 0.000009I_pT_{on} + 0.000006I_pA_p + 0.0000004833T_{on}A_p \quad (5)$$

$$REW = 0.001464 - 0.000017T_{on} - 0.000879I_p + 0.000023A_p + 0.000222I_p^2 + 0.000002A_p^2 + 0.0000001431T_{on}^2 + 0.000005I_pT_{on} - 0.00002I_pA_p - 0.00000039T_{on}A_p \quad (6)$$

$$R_a = 2.25398 - 0.00513426T_{on} - 0.17375I_p - 0.0236667A_p + 0.0633333I_p^2 + 0.00000925926T_{on}^2 + 0.000758333A_p^2 + 0.004I_pT_{on} - 0.00175I_pA_p - 0.000125T_{on}A_p \quad (7)$$

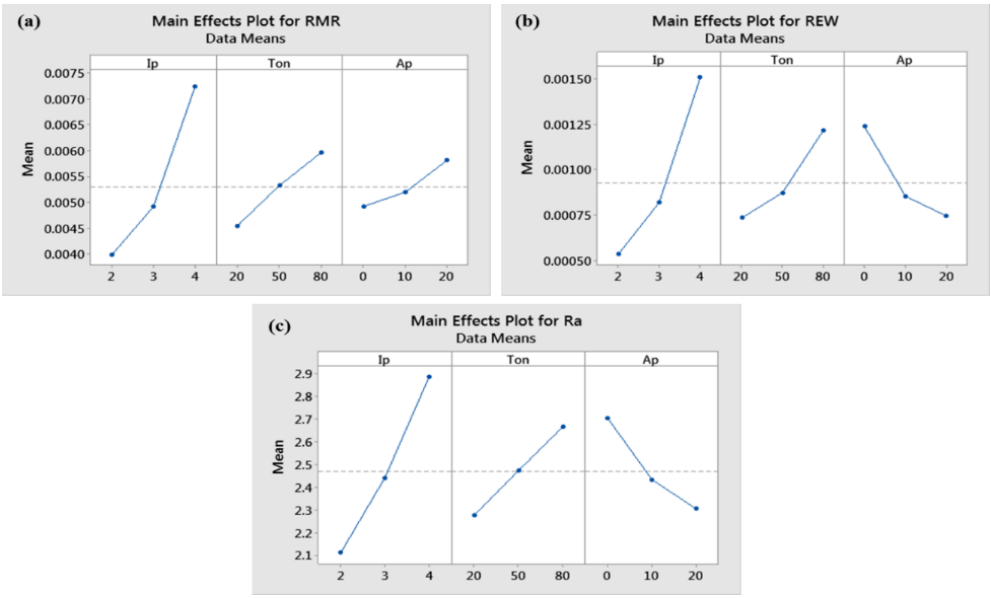

Figure 2. Main influential plot of machining parameters on (a) RMR, (b) REW, and (c) R_a.

The normal probability plots described in Figures 3a-c indicate that the residuals lie on the reference lines with little deviations dispersed around a steep line. Therefore, the model terms selected are the only major variables, and their errors have the form of a normal distribution [19]. The development models were also considered for appraising the adequacy via ANOVA analysis in the following sections for predicting the optimum attributes.

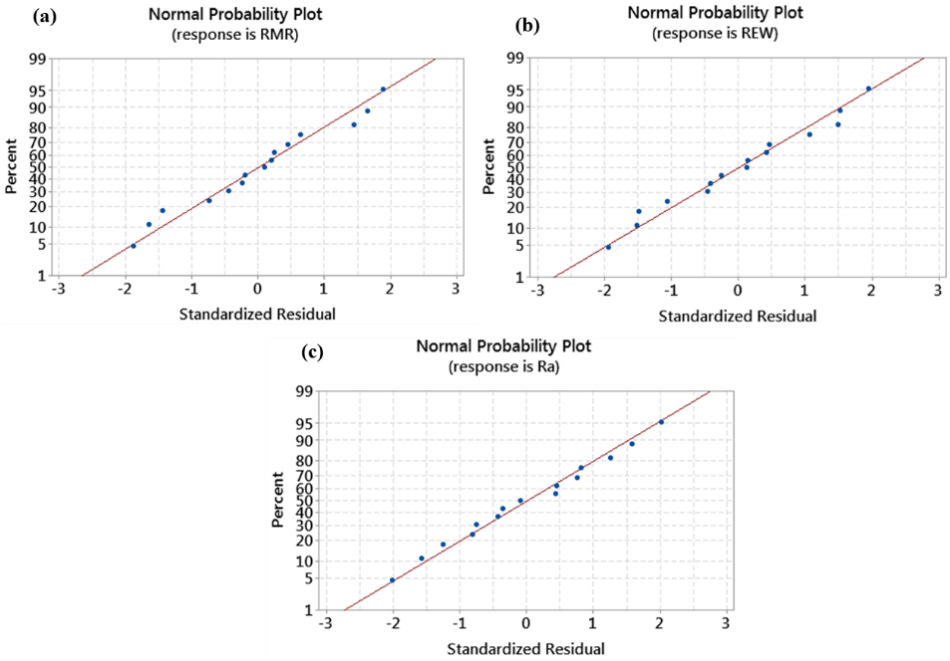

Figure 3. Normal probability plot: (a) RMR, (b) REW, and (c) R_a.

3.2. Investigation of RMR results

3.2.1. ANOVA analysis

The RMR model was evaluated for its adequacy via ANOVA analysis, with a confidence level of 95 % and a significance level of 5 %. Table 2 shows the ANOVA results of RMR. The P-values corresponding to the model terms are significant when they are smaller than 5 %. Hence, the terms (comprising T_{on}, I_p, A_p, I_p^2) are significant for the RMR model. The development model has been confirmed by the precision/adequacy through coefficients, including "R^2", "R^2(adj)", and "R^2(pred)". In which, the R^2 value is 0.9895. The empirical and predictive values reveal that they have good consistency. The R^2(pred) value is 0.8511, which is also in agreement with the R^2(adj) value of 0.9707.

Table 2. ANOVA for RMR model.

	Sum of squares	Mean square	F-value	p-value	Remark	Contribution
Model	2.924E-05	3.249E-06	52.55	0.0002031	significant	
I_p	2.126E-05	2.126E-05	343.9	8.391E-06	significant	71.95 %
T_{on}	4.033E-06	4.033E-06	65.23	0.0004715	significant	13.65 %
A_p	1.586E-06	1.586E-06	25.65	0.003884	significant	5.37 %
I_p x T_{on}	2.809E-07	2.809E-07	4.543	0.08624	not significant	6.09 %

I_p x A_p	1.464E-08	1.464E-08	0.2368	0.6471	not significant	0.00 %
T_{on} x A_p	8.410E-08	8.410E-08	1.360	0.2961	not significant	0.61 %
I_p^2	1.863E-06	1.863E-06	30.13	0.002740	significant	0.95 %
T_{on}^2	2.308E-13	2.308E-13	3.732E-06	0.9985	not significant	0.05 %
A_p^2	1.791E-07	1.791E-07	2.897	0.1495	not significant	0.28 %
Lack of fit	2.693E-07	8.978E-08	4.512	0.0563	not significant	0.91 %
"R^2" = 0.9895, " R^2(adj)" = 0.9707, and "R^2(pred)" = 0.8511						

3.2.2. Influences of process parameters on RMR

The incorporated influence of process parameters on RMR is disclosed in Figure 4. In which I_p expresses the most influence on RMR with a contribution of 71.95 %, followed by T_{on} (13.65 %) and A_p (5.37 %), as indicated in Table 2. As a result, RMR augments with an increase of I_p in the entire investigation spaces of A_p and T_{on}. Moreover, RMR rises (or decreases) with an augmentation in A_p (or T_{on}) for the whole design spaces of I_p.

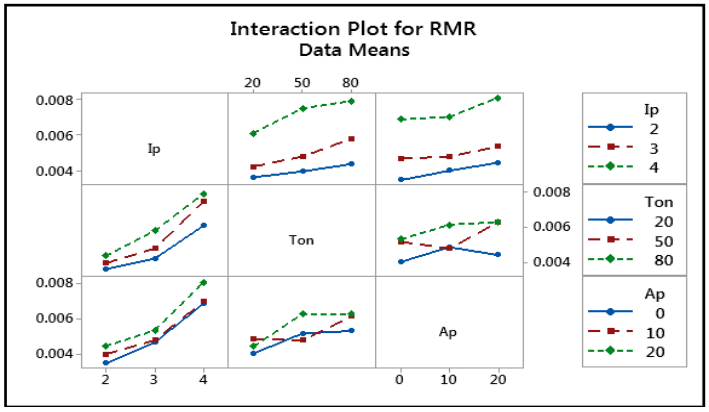

Figure 4. Interaction influence plots of variables for RMR.

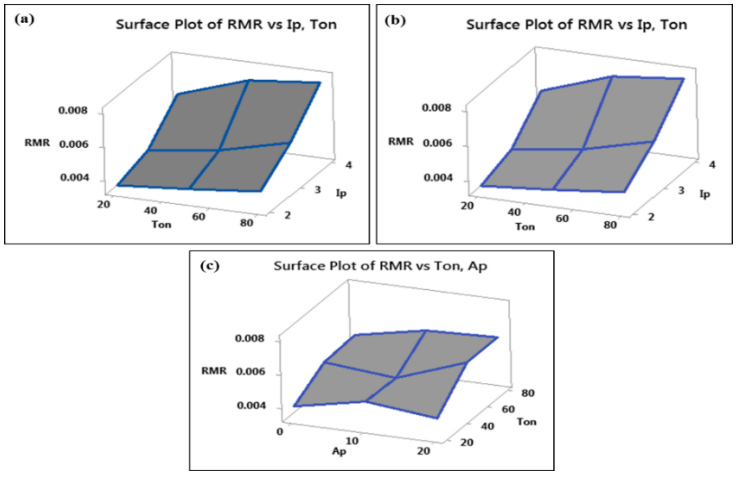

Figure 5. 3D surface plots for RMR: (a) I_p vs T_{on}; (b) I_p vs A_p; (c) T_{on} vs A_p.

Figures 5a–c show the 3D surface plots of RMR when one factor is fixed while the other two factors are varied. In Figure 8a, an upward tendency of RMR is expressed when T_{on} and I_p increase simultaneously. A sudden drop in RMR is observed at I_p of 3 A and T_{on} of 50 µs. RMR

obtains the largest value at I_p of 4 A and T_{on} of 80 μs, and the smallest value at I_p of 2 A and T_{on} of 20 μs. Observing Figure 5b, RMR improves as both A_p and I_p increase. An unusual decrease in RMR is confirmed at I_p of 3 A and A_p of 10 g/L. RMR augments at a powder amount of 20 g/L for all I_p values, whilst it degrades at a powder amount of 0 g/L for all I_p values. The intersections of (I_p = 2 A, A_p = 0 g/L) and (I_p = 4 A, A_p = 20 g/L) disclose the smallest and largest RMR, respectively. In Figure 5c, an upward tendency of RMR is observed when T_{on} increases with the augmentation of A_p. An uncommon decrease in RMR is affirmed at T_{on} of 50 μs and A_p of 10 g/L. The intersections of (T_{on} = 20 μs, A_p = 0 g/L) and (T_{on} = 80 μs, A_p = 20 g/L) depict the smallest and largest RMR, respectively.

The above analysis indicates that increasing both T_{on} and I_p raises discharge energy, thereby improving RMR [20]. However, excessive energy input may cause unstable machining due to insufficient debris removal in the discharge gap, resulting in short circuits [21]. The introduction of powder into the dielectric promotes dispersed discharges, which enhances RMR. Conversely, a reduction in RMR may occur due to short circuits, arc formation caused by excessive debris from previous discharges, or an inappropriate combination of I_p and T_{on} that reduces powder concentration during subsequent discharges [22]. The RMR results obtained with tungsten compound powder are consistent with previous studies [23, 24], although different process parameters and powder types were used.

3.3. Investigation of REW results

3.3.1. ANOVA analysis

The REW model was considered for evaluating its adequation through ANOVA analysis with a confidence level of 95 % and a significance level of 5 %. The ANOVA results of the REW model are shown in Table 3. The P-values corresponding to the model terms are significant when they are less than 5 %. Accordingly, the terms A_p, I_p, I_p^2, I_pxA_p, and A_p^2 are significant. The developed model has been confirmed by the precision/adequacy through coefficients, including "R^2", "R^2(adj)" and "R^2(pred)". In which, the R^2 value is 0.9947, indicating that the empirical and predictive values show a good compromise. The R^2(pred) value is 0.9145, which is also suitable with the R^2(adj) value of 0.985.

Table 3. ANOVA results for REW model.

	Sum of squares	Mean square	F-value	P-value	Remark	Contribution
Model	3.749E-05	4.17E-06	103.2	< 0.0001	significant	
I_p	2.528E-05	2.53E-05	626.3	< 0.0001	significant	67.13 %
T_{on}	6.390E-08	6.390E-08	1.583	0.2638	not significant	0.17 %
A_p	5.623E-07	5.623E-07	13.93	0.01353	significant	1.49 %
I_p x T_{on}	1.884E-07	1.884E-07	4.667	0.08316	not significant	0.5 %
I_p x A_p	2.025E-06	2.025E-06	50.17	0.0008682	significant	5.38 %
T_{on} xA_p	2.176E-08	2.176E-08	0.5390	0.4958	not significant	0.06 %
I_p^2	8.206E-06	8.206E-06	203.3	< 0.0001	significant	21.46 %
T_{on}^2	2.592E-07	2.592E-07	6.422	0.05226	not significant	0.93 %
A_p^2	8.994E-07	8.994E-07	22.28	0.005240	significant	2.35 %
Lack of Fit	2.014E-07	6.714E-08	364.3	0.002739	significant	0.53 %
"R^2" = 0.9947, "R^2(adj)" = 0.985, and "R^2 (Pred)" = 0.9145						

3.3.2. Influences of process parameters on REW

Figure 6 indicates the incorporated influence of machining variables on REW. According to the ANOVA results of REW given in Table 3, I_p expresses the most contribution for REW with 67.13 %, followed by A_p (1.49 %) and T_{on} (0.17 %). As the results of the incorporated impact plots shown in Figure 6, REW augments with an increase of I_p in the whole investigation spaces of T_{on} and A_p. Additionally, REW grows (or decreases) with an increment in A_p (or T_{on}) in the entire investigation spaces of I_p.

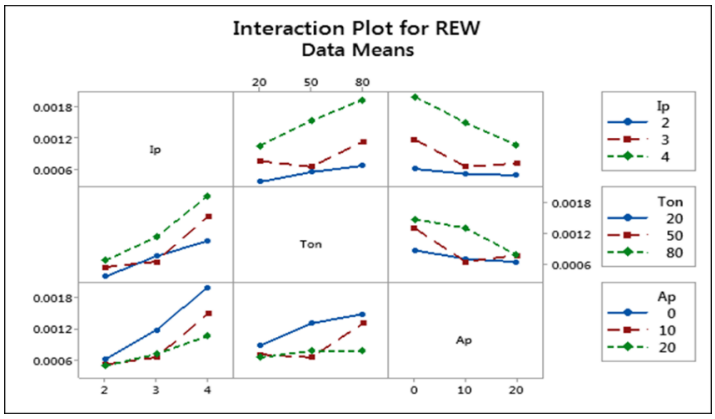

Figure 6. Interaction influence plots of variables for REW.

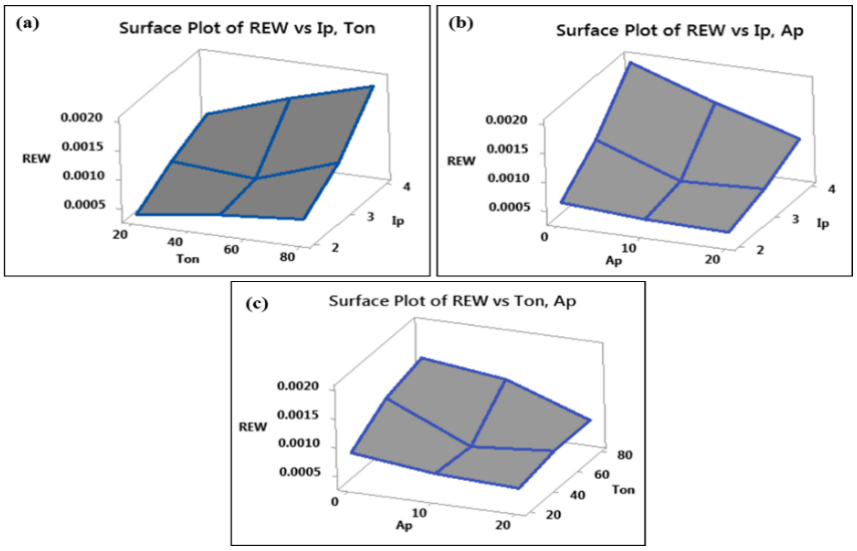

Figure 7. 3D surface plots for REW: (a) I_p vs T_{on}; (b) I_p vs A_p; (c) T_{on} vs A_p.

The 3D surface plots of REW when one factor is fixed while the other two factors are altered are presented in Figures 7a–c. Specifically, in Figure 7a, an upward tendency of REW is disclosed with the boost of both I_p and T_{on}. A rapid decline in REW is observed at I_p of 3 A and T_{on} of 50 µs. At I_p of 4 A and T_{on} of 80 µs, REW attains the greatest value, while at I_p of 2 A and T_{on} of 20 µs, it reaches the smallest value. It is clear from Figure 7b that REW declines with the increase of both A_p and I_p. An unusual drop in REW is verified at I_p of 3 A and A_p of 10 g/L. REW degrades at a powder amount of 20 g/L for all I_p values, whilst it augments at a powder amount of 0 g/L for all I_p values. The intersections of (I_p = 4 A, A_p = 0 g/L) and (I_p = 2 A, A_p =

20 g/L) reveal the largest and smallest REW, respectively. In general, as can be seen from Figure 7c, a downward tendency of REW is indicated when the pulse on time drops with the augmentation of the powder amount. An uncommon decrease in REW is confirmed at T_{on} of 50 µs and A_p of 10 g/L. The intersections of (T_{on} = 20 µs, A_p = 20 g/L) and (T_{on} = 80 µs, A_p = 0 g/L) depict the smallest and largest REW, respectively.

The above analysis indicates that increasing both I_p and T_{on} enhances discharge energy, causing more heat to be transferred to the electrode and consequently increasing REW [13]. However, excessive energy input may destabilize the process due to ineffective debris removal in the discharge gap, resulting in short circuits. The presence of powder in the dielectric promotes dispersed discharges, which can increase REW [25]. Conversely, abnormal reductions in REW may occur due to short circuits or arc formation caused by excessive debris accumulation from previous discharges [26]. Furthermore, an unsuitable combination T_{on} and I_p generates high bubble collapse pressure, reducing powder concentration in subsequent discharges. This decreases discharge energy and heat transferred to the electrode, leading to lower REW. The REW behavior is consistent with previous studies [24, 27], although its dependence on process parameters varies with electrical conditions and the thermal-electrical properties of different powders.

3.4. Investigation of R_a results

3.4.1. ANOVA analysis

The ANOVA analysis with a confidence level of 95 % and a significance level of 5 % was utilized to evaluate the suitability of the R_a model, the results of which are given in Table 4. The P-values corresponding to the model terms are significant when they are less than 5 %. Accordingly, the significant terms of the R_a model are T_{on}, I_p, A_p, I_p^2, A_p^2, and I_p x T_{on}. The developed model has been confirmed by the precision/adequacy through coefficients, including "R^2", "R^2(adj)" and "R^2(pred)". In which, the R^2 value is 0.9947, demonstrating that the empirical and predictive values show a good compromise. The R^2(pred) and R^2(adj) values are 0.9166 and 0.9848, respectively. This indicates that there is a suitable agreement between "R^2(pred)" and "R^2(adj)".

Table 4. ANOVA results for R_a model.

	Sum of squares	Mean square	F-value	P-value	Remark	Contribution
Model	1.935	0.2150	102.0	< 0.0001	significant	
I_p	1.209	1.209	573.4	< 0.0001	significant	62.20 %
T_{on}	0.3081	0.3081	146.1	< 0.0001	significant	15.85 %
A_p	0.3200	0.3200	151.8	< 0.0001	significant	14.46 %
I_p x T_{on}	0.05760	0.05760	27.32	0.003391	significant	2.96 %
I_p x A_p	0.001225	0.001225	0.5810	0.4803	not significant	0.06 %
T_{on} x A_p	0.005625	0.005625	2.668	0.1633	not significant	0.29 %
I_p^2	0.01481	0.01481	7.025	0.04540	significant	0.60 %
T_{on}^2	0.0002564	0.0002564	0.1216	0.7415	not significant	0.00 %
A_p^2	0.02123	0.02123	10.07	0.02472	significant	1.04 %
Lack of fit	0.01008	0.003358	14.39	0.06566	not significant	0.52 %
"R^2" = 0.9947, "R^2(adj)" = 0.9848, and "R^2(Pred)" = 0.9166						

3.4.2. Influences of processing parameters on R_a

Figure 8 indicates the incorporated influence of machining variables on the roughness. I_p has the greatest influence on R_a with a contribution rate of 62.20 %, followed by T_{on} (15.85 %) and A_p (14.46 %), according to the ANOVA results shown in Table 4. From the results of the incorporated effect plots (Figure 8), R_a rises with an augmentation of T_{on} and I_p in the entire investigation spaces of A_p. Meanwhile, R_a declines with an augmentation of A_p in the entire investigation spaces of T_{on} and I_p. These observations are suitable to the outcomes previously announced [28, 29].

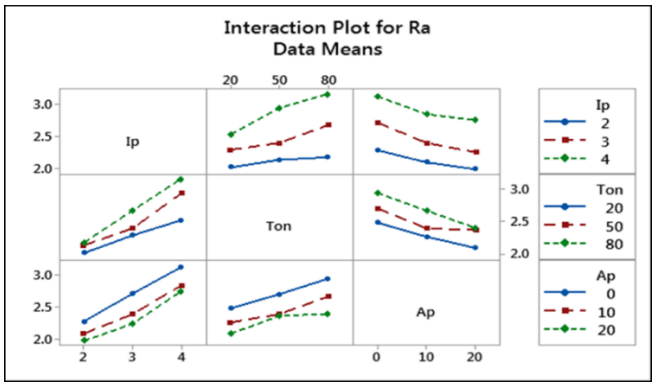

Figure 8. Interaction influence plots of variables for R_a.

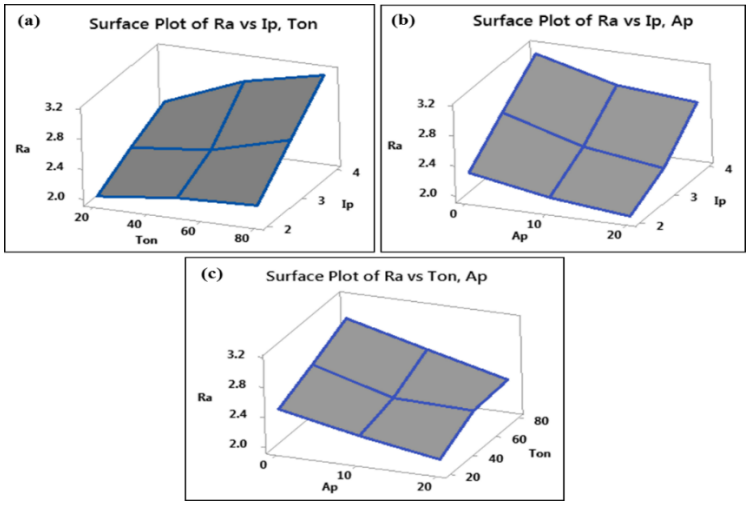

Figure 9. 3D surface plots for R_a: (a) I_p vs T_{on}; (b) I_p vs A_p; (c) T_{on} vs A_p.

Figures 9a–c illustrate the 3D surface plots of R_a with one factor held fixed while the other two factors are mutated. Specifically, in Figure 9a, an upward trend of R_a is described by the increase of both I_p and T_{on}. A sudden decline in R_a is observed at I_p of 3 A and T_{on} of 50 µs. At I_p of 4 A and T_{on} of 80 µs, R_a achieves the greatest value, while at I_p of 2 A and T_{on} of 20 µs, it reaches the smallest value. In Figure 9b, it is easy to see that R_a declines with the increase of both A_p and I_p. An unusual drop in R_a is verified at I_p of 3 A and A_p of 10 g/L. R_a degrades at a powder amount of 20 g/L for all I_p values, whilst it augments at a powder amount of 0 g/L for all I_p values. The intersections of (I_p = 4 A, A_p = 0 g/L) and (I_p = 2 A, A_p = 20 g/L) reveal the largest and smallest R_a, respectively. In general, as can be seen from Figure 9c, a downward

tendency of R_a is observed when T_{on} drops with the augmentation of A_p. An uncommon decrease in R_a is confirmed at T_{on} of 50 µs and A_p of 10 g/L. The intersections of (T_{on} = 20 µs, A_p = 20 g/L) and (T_{on} = 80 µs, A_p = 0 g/L) depict the smallest and largest R_a, respectively.

The analysis shows that increasing both I_p and T_{on} raises discharge energy, resulting in higher R_a values [13]. However, excessive energy input may cause unstable machining due to insufficient debris removal, leading to short circuits or arcing [30]. The addition of powder into the dielectric promotes dispersed discharges and enlarges the discharge gap, which reduces discharge energy density and produces smaller surface craters, thereby improving R_a. Conversely, abnormal R_a deterioration may occur due to short circuits, arcing from excessive debris accumulation, or an inappropriate combination of I_p and T_{on} that decreases powder concentration during subsequent discharges [31]. In this study, PMEDM produced higher R_a values than EDM across the investigated range, and the trend agrees with previous studies [32, 33]. However, the influence of powder addition depends on the thermal and electrical properties of the powder, dielectric fluid, and machining parameters.

3.5. Optimization outcomes of machining features

The multi-criteria optimization problem of this study is described as follows:

Finding x = [T_{on}, I_p, A_p] such that RMR and {REW and R_a} simultaneously reach their respective maximum and minimum values using TOPSIS and DA algorithms, as shown in [27].

The process parameters are within the following conditions: $20 \leq T_{on} \leq 80$ (µs), $2 \leq I_p \leq 4$ (A), and $0 \leq A_p \leq 20$ (g/L).

The entropy weight approach was used to determine the weights of the three responses, resulting in $w_1 = 0.249$ for RMR, $w_2 = 0.680$for REW, and $w_3 = 0.072$ for R_a, which was computed according to reference [15]. The optimal condition obtained from TOPSIS was the 15th experimental run with $I_p = 2$A, $T_{on} = 50$µs, and $A_p = 20$g/L, achieving R_a = 1.98 µm, RMR = 0.00446 g/min, and REW = 0.00049 g/min (Table 5). Using the same weighting factors, the DA method identified the optimal parameters as $I_p = 2$A, $T_{on} = 70$µs, and $A_p = 20$g/L with a desirability value of 0.878, producing R_a = 1.99 µm, RMR = 0.004847 g/min, and REW = 0.0005445 g/min (Table 5). Compared with DA, TOPSIS provided lower REW and R_a by 10 % and 0.5 %, respectively, while DA achieved 8.67% higher RMR (Table 5). Therefore, TOPSIS is more suitable when minimizing REW and R_a is prioritized, whereas DA is preferable for maximizing RMR.

Table 5. Comparison of optimal results.

Algorithm	Optimal variables			Machining attributes		
	T_{on} (µs)	I_p (A)	A_p (g/L)	RMR (g/min)	REW (g/min)	R_a (µm)
DA	70	2	20	0.004847	0.0005445	1.99
TOPSIS	50	2	20	0.00446	0.00049	1.98
Comparison between TOPSIS and DA				↑ 8.67 %	↓ 10 %	↓ 0.5 %

3.6. Empirical verification of the results

The experimental values of machining responses at the optimal parameters are depicted in Table 6. The errors between the values of output variables for the empirical and predicted

models are within the tolerable assortment, with the largest error of 6.3 % for REW and the smallest error of 2.2 % for R_a, both obtained by the TOPSIS technique.

Table 6. Empirical verification of the results.

Algorithm	Machining attributes	Optimum variables	PV	EV	Error (%)
DA	RMR, g/min	I_p = 2 A, T_{on} = 70 µs, A_p = 20 g/L	0.004847	0.004561	5.9
	REW, g/min		0.0005445	0.000524	3.8
	R_a, µm		1.99	2.05	2.9
TOPSIS	RMR, g/min	I_p = 2 A, T_{on} = 50 µs, A_p = 20 g/L	0.00446	0.004339	2.7
	REW, g/min		0.00049	0.00052	6.3
	R_a, µm		1.98	2.02	2.2

Error = Abs (PV − EV)/PV×100 %

The surface defects under the optimal conditions obtained from the two algorithms were analyzed, as shown in Figure 10. Figures 10a and 10b present the surface morphology corresponding to the TOPSIS and DA methods, respectively. It can be observed that defects, including droplets, debris particles, micro-cracks, and voids, are less pronounced in the TOPSIS condition than in the DA condition. Since both methods use the same I_p and A_p, the higher T_{on} value from the DA method contributes to the formation of more surface defects [33]. This phenomenon is related to the involvement of powder particles in the discharge process, which promotes dispersed discharges, alters material removal behavior, generates residual stresses, and affects dielectric properties such as viscosity, conductivity, and heat transfer [34]. The defect density observed in this study is higher than that reported in previous work [10], which can be attributed to the present investigation focusing on heat-treated material, whereas the previous study examined the non-heat-treated state.

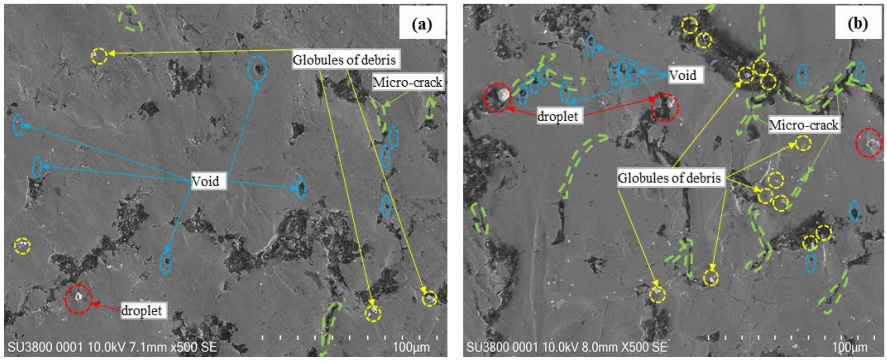

Figure 10. Surface defects at optimal parameters: (a) TOPSIS; (b) DA.

The surface chemical compositions obtained under the optimal conditions of TOPSIS and DA were compared, as presented in Table 7. The results show that the concentrations of C, W, Co, and Cu from the TOPSIS condition are higher than those from DA, whereas the contents of V, Si, Cr, Fe, and Mo are greater under the DA condition. This difference is attributed to the distinct optimal parameters selected by the two optimization methods, which generate different physical and chemical interactions during the discharge process. Additionally, the element O was not detected on the machined surfaces produced by either method. The elemental distributions under the optimal TOPSIS and DA conditions are illustrated in Figure 11. The TOPSIS condition exhibits a more uniform distribution of elements compared with the DA

condition. This variation is related to the different parameter combinations, which influence the discharge channel characteristics and consequently the material transfer and surface modification mechanisms [35]. Although the elemental composition differs from previous research [10], both studies confirm the diffusion of W elements and the formation of the W_2C phase on the machined surface.

Table 7. Chemical composition and elemental content on surfaces at optimal parameters.

Algorithm	Chemical elements (wt.%)								
	C	V	Si	Cr	Fe	Mo	W	Co	Cu
DA	19.42	1.25	0.85	5.39	68.61	2.40	1.70	0.33	0.28
TOPSIS	21.9	1.22	0.59	4.35	59.43	2.34	9.34	0.44	0.39

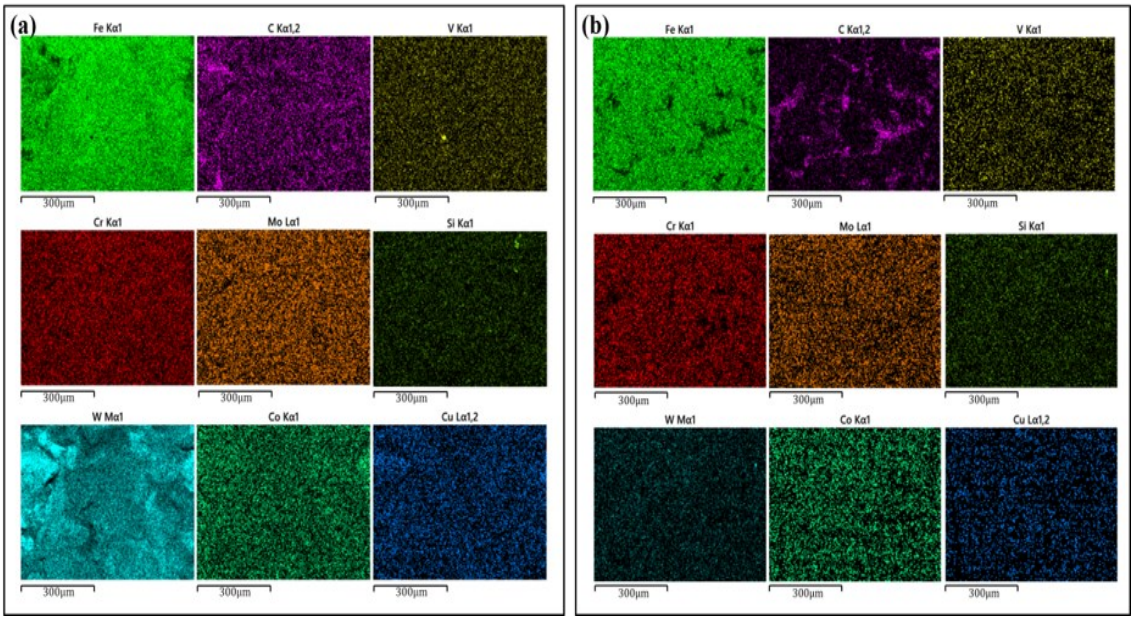

Figure 11. Distribution of chemical elements on surfaces at optimal parameters : (a) TOPSIS and (b) DA.

Regarding the recast layer, the TRL obtained from the TOPSIS method is thinner than that from the DA method, as shown in Figures 12a and 13. The surface layer produced under the optimal TOPSIS condition exhibits a more uniform distribution of tungsten carbide phases compared with the DA condition. Moreover, the CAP value achieved by TOPSIS is lower than that obtained by DA (Figure 12b). These differences are mainly attributed to the different electrical parameters selected by the two optimization methods, which affect the decomposition pressure of gas bubbles during previous discharges and the role of powder particles in subsequent discharges [36]. The presence of an appropriate powder concentration promotes stable and uniform discharge channels with a wider discharge area [26]. Furthermore, the dielectric fluid with suspended powder reduces viscosity, enhancing debris removal from the discharge zone. These effects contribute to the reduction of TRL and CAP. The surface topographies under the optimal TOPSIS and DA conditions are presented in Figures 14a and 14b, respectively. The TOPSIS condition produces a more uniform surface morphology, whereas the DA condition shows a less homogeneous surface structure.

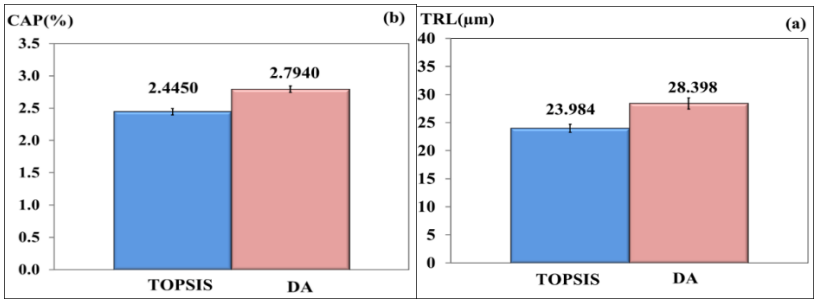

Figure 12. TRL and CAP at optimal parameters: (a) TRL; (b) CAP.

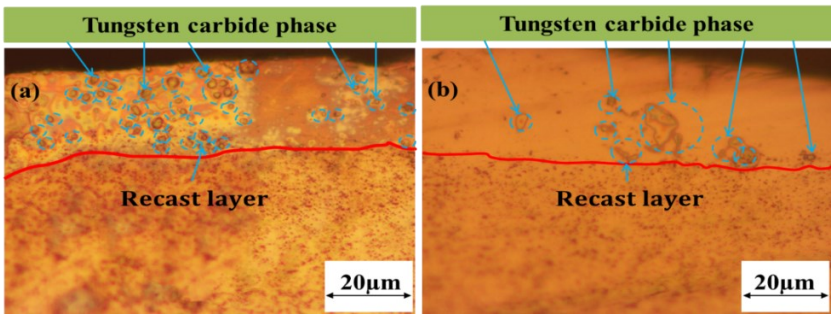

Figure 13. Recast layer at optimal parameters: (a) TOPSIS; (b) DA.

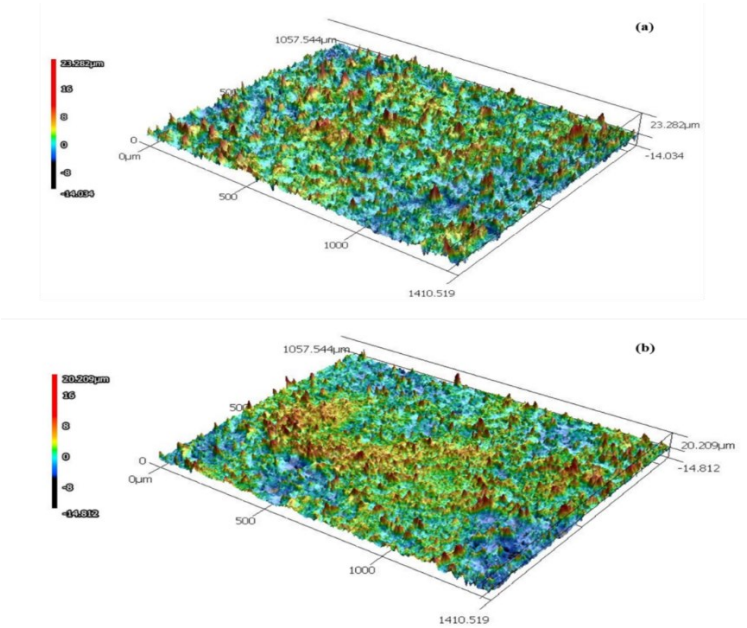

Figure 14. Surface topography of specimens at optimal parameters: (a) TOPSIS; (b) DA.

4. CONCLUSIONS

In this study, the machinability of heat-treated SKD61 steel in EDM operations with tungsten compound powder was evaluated. The principal results have been drawn:

- The predictive models with well-reliability have been instituted, with the R^2-values of RMR, REW, and R_a are 0.9895, 0.9947 and 0.9947, respectively. An upward of I_p or T_{on} leads to an increment in entire output attributes. For A_p, an augmentation in A_p leads to an increment in RMR and a reduction of REW and R_a. For RMR, the influence of I_p is the greatest with a contribution rate of 71.95 %, followed by T_{on} and A_p corresponding to a contribution rate of 13.65 % and 5.37 %. For REW, the greatest impact on REW is I_p with a contribution rate of 67.13 %, followed by A_p with a contribution rate of 1.49 %, and T_{on} with a contribution rate of 0.17 %. For R_a, I_p has also the greatest impact on R_a with a contribution rate of 62.2 %, followed by T_{on} with a contribution rate of 15.85 %, and A_p with a contribution rate of 14.46 %.

- Both the TOPSIS and DA were employed to solve the multi-criteria optimization problem. DA gives the best result in terms of improving RMR with an increment of 8.67 % compared to TOPSIS. Meanwhile, TOPSIS contributes the most suitable outcome for reducing REW and R_a with corresponding reductions of 10 % and 0.5 % compared to DA. The defects, TRL, CAP, and surface topography of TOPSIS are better improved than those of DA. The content of elements such as C, W, Co, and Cu of TOPSIS is larger compared to that of DA, whilst the content of elements such as Si, V, Fe, Cr, and Mo of DA is also more than that of TOPSIS. For the distribution of chemical composition, as well as the distribution of W_2C, TOPSIS has better results than DA. Hence, the chosen approach will depend on the requirements for surface feature criteria or machining ability criteria.

- The findings of this study provide a more comprehensive knowledge of machinability of heat-treated SKD61 steel in the EDM operation with tungsten compound powder, and the benefits of the DA and TOPSIS algorithms. These factors can help foster the well-being of industrial production and the research community.

Acknowledgements. This research is funded by the Vietnam National Foundation for Science and Technology Development (NAFOSTED) under grant number 107.99-2021.29.

CRediT authorship contribution statement. Van-Tao Le: Conceptualization, Methodology, Investigation, Writing - original draft, Writing - review & editing, Funding acquisition. Thi Hong Minh Nguyen, Tien Dung Hoang: Investigation, Writing - original draft.

Declaration of competing interest. The authors declare that they have no conflicts of interest.

REFERENCES

1. Askeland D. R. – The science and engineering of materials, Springer US, Boston, MA (1996). https://doi.org/10.1007/978-1-4899-2895-5.
2. Hu P., Ying L., He B. – Hot stamping advanced manufacturing technology of lightweight car body, Springer Singapore, Singapore (2017). https://doi.org/10.1007/978-981-10-2401-6.
3. Jahan M. P. – Electrical discharge machining (EDM) types, technologies and applications, Nova, New York (2015).
4. Srivastava S., Vishnoi M., Gangadhar M. T., Kukshal V. – An insight on powder mixed electric discharge machining: A state of the art review. Proc. Inst. Mech. Eng. Part B J. Eng. Manuf., **237** (2022) 657–690. https://doi.org/10.1177/09544054221111896.
5. Philip J. T., Mathew J., Kuriachen B. – Transition from EDM to PMEDM - impact of suspended particulates in the dielectric on Ti6Al4V and other distinct material surfaces: A review. J. Manuf. Process., **64** (2021) 1105–1142. https://doi.org/10.1016/j.jmapro.2021.01.056.

6. Wu K. L., Yan B. H., Huang F. Y., Chen S. C. – Improvement of surface finish on SKD steel using electro-discharge machining with aluminum and surfactant added dielectric. Int. J. Mach. Tools Manuf., **45** (2005) 1195–1201. https://doi.org/10.1016/j.ijmachtools.2004.12.005.
7. Yan B., Lin Y., Huang F., Wang C. – Surface modification of SKD 61 during EDM with metal powder in the dielectric. Mater. Trans., **42** (2001) 2597–2604. https://doi.org/10.2320/matertrans.42.2597.
8. Amorim F. L., Dalcin V. A., Soares P., Mendes L. A. – Surface modification of tool steel by electrical discharge machining with molybdenum powder mixed in dielectric fluid. Int. J. Adv. Manuf. Technol., **91** (2017) 341–350. https://doi.org/10.1007/s00170-016-9678-x.
9. Peças P., Henriques E. – Influence of silicon powder-mixed dielectric on conventional electrical discharge machining. Int. J. Mach. Tools Manuf., **43** (2003) 1465–1471. https://doi.org/10.1016/S0890-6955(03)00169-X.
10. Kumar S., Batra U. – Surface modification of die steel materials by EDM method using tungsten powder-mixed dielectric. J. Manuf. Process., **14** (2012) 35–40. https://doi.org/10.1016/j.jmapro.2011.09.002.
11. Zhang H., Choi J. P., Moon S. K., Ngo T. H. – A hybrid multi-objective optimization of aerosol jet printing process via response surface methodology. Addit. Manuf., **33** (2020) 101096. https://doi.org/10.1016/j.addma.2020.101096.
12. Ishfaq K., Waseem M. U. – Cutting performance evaluation of modified dielectrics in nano powder mixed electric discharge machining (NPMEDM) of Ni-based super alloy. CIRP J. Manuf. Sci. Technol., **41** (2023) 196–215. https://doi.org/10.1016/j.cirpj.2022.11.018.
13. Fazli Shahri H. R., Mahdavinejad R., Ashjaee M., Abdullah A. – A comparative investigation on temperature distribution in electric discharge machining process through analytical, numerical and experimental methods. Int. J. Mach. Tools Manuf., **114** (2017) 35–53. https://doi.org/10.1016/j.ijmachtools.2016.12.005.
14. Le V. T. – The evaluation of machining performances and recast layer properties of AISI H13 steel processed by tungsten carbide powder mixed EDM process in the semi-finishing process. Mach. Sci. Technol., **26** (2022) 428–459. https://doi.org/10.1080/10910344.2022.2129983.
15. Li X., Wang K., Liu L., Xin J., Yang H., Gao C. – Application of the entropy weight and TOPSIS method in safety evaluation of coal mines. Procedia Eng., **26** (2011) 2085–2091. https://doi.org/10.1016/j.proeng.2011.11.2410.
16. Pachaury Y., Tandon P. – An overview of electric discharge machining of ceramics and ceramic based composites. J. Manuf. Process., **25** (2017) 369–390. https://doi.org/10.1016/j.jmapro.2016.12.010.
17. Öpöz T. T., Yaşar H., Ekmekci N., Ekmekci B. – Particle migration and surface modification on Ti6Al4V in SiC powder mixed electrical discharge machining. J. Manuf. Process., **31** (2018) 744–758. https://doi.org/10.1016/j.jmapro.2018.01.002.
18. Chen S. L., Lin M. H., Huang G. X., Wang C. C. – Research of the recast layer on implant surface modified by micro-current electrical discharge machining using deionized water mixed with titanium powder as dielectric solvent. Appl. Surf. Sci., **311** (2014) 47–53. https://doi.org/10.1016/j.apsusc.2014.04.204.
19. Akpan E. S., Dauda M., Kuburi L. S., Obada D. O. – Box-Behnken experimental design for the process optimization of catfish bones derived hydroxyapatite: A pedagogical approach. Mater. Chem. Phys., **272** (2021) 124916. https://doi.org/10.1016/j.matchemphys.2021.124916.
20. Ho K. H., Newman S. T. – State of the art electrical discharge machining (EDM). Int. J. Mach. Tools Manuf., **43** (2003) 1287–1300. https://doi.org/10.1016/S0890-6955(03)00162-7.
21. Jithin S., Raut A., Bhandarkar U. V., Joshi S. S. – Finite element model for topography prediction of electrical discharge textured surfaces considering multi-discharge phenomenon. Int. J. Mech. Sci., **177** (2020) 105604. https://doi.org/10.1016/j.ijmecsci.2020.105604.
22. Le V. T. – The influence of additive powder on machinability and surface integrity of SKD61 steel by EDM process. Mater. Manuf. Process., **36** (2021) 1084–1098. https://doi.org/10.1080/10426914.2021.1885710.

23. Sahu S. K., Jadam T., Datta S., Nandi G. – Effect of using SiC powder-added dielectric media during electro-discharge machining of Inconel 718 superalloys. J. Braz. Soc. Mech. Sci. Eng., **40** (2018) 330. https://doi.org/10.1007/s40430-018-1257-7.
24. Shabgard M., Khosrozadeh B. – Investigation of carbon nanotube added dielectric on the surface characteristics and machining performance of Ti-6Al-4V alloy in EDM process. J. Manuf. Process., **25** (2017) 212–219. https://doi.org/10.1016/j.jmapro.2016.11.016.
25. Ekmekci B., Yaşar H., Ekmekci N. – A discharge separation model for powder mixed electrical discharge machining. J. Manuf. Sci. Eng., **138** (2016) 1–9. https://doi.org/10.1115/1.4033042.
26. Furutania K., Saneto A., Takezawa H., Mohri N., Miyake H. – Accretion of titanium carbide by electrical discharge machining with powder suspended in working fluid. Precis. Eng., **25** (2001) 138–144. https://doi.org/10.1016/s0141-6359(00)00068-4.
27. Le V. T., Hoang L., Ghazali M. F., Le V. T., Do M. T., Nguyen T. T., Vu T. S. – Optimization and comparison of machining characteristics of SKD61 steel in powder-mixed EDM process by TOPSIS and desirability approach. Int. J. Adv. Manuf. Technol., **130** (2024) 403–424. https://doi.org/10.1007/s00170-023-12680-8.
28. Jadam T., Sahu S. K., Datta S., Masanta M. – EDM performance of Inconel 718 superalloy: Application of multi-walled carbon nanotube (MWCNT) added dielectric media. J. Braz. Soc. Mech. Sci. Eng., **41** (2019) 305. https://doi.org/10.1007/s40430-019-1813-9.
29. Paswan K., Pramanik A., Chattopadhyaya S. – Machining performance of Inconel 718 using graphene nanofluid in EDM. Mater. Manuf. Process., **35** (2020) 33–42. https://doi.org/10.1080/10426914.2020.1711924.
30. Le V. T. – The role of electrical parameters in adding powder influences the surface properties of SKD61 steel in EDM process. J. Braz. Soc. Mech. Sci. Eng., **43** (2021) 120. https://doi.org/10.1007/s40430-021-02844-6.
31. Le, V.-T., Nguyen, T.H.M., Hoang, T.D., Nguyen, V.S. – Novel insights for machining and metallurgical surface features of the heat treatment and non-heat treatment X40CrMoV51 tool steel by powder-added EDM process. Int. J. Adv. Manuf. Technol., **137** (2025) 4063–4088. https://doi.org/10.1007/s00170-025-15396-z.
32. Le V. – New insights into the surface features of SKD61 steel at heat-treated and non-heat-treated states as processed by powder-mixed EDM. Mater. Lett., **352** (2023) 135199. https://doi.org/10.1016/j.matlet.2023.135199.
33. Dubey V., Sharma A. K., Singh B. – Optimization of machining parameters in chromium-additive mixed electrical discharge machining of the AA7075/5%B_4C composite. Proc. Inst. Mech. Eng. Part E J. Process Mech. Eng., **236** (2022) 104–113. https://doi.org/10.1177/09544089211031755.
34. Lee S. H., Li X. – Study of the surface integrity of the machined workpiece in the EDM of tungsten carbide. J. Mater. Process. Technol., **139** (2003) 315–321. https://doi.org/10.1016/S0924-0136(03)00547-8.
35. Davis R., Singh A., Debnath K., Sabino R. M., Popat K., da Silva L. R. R., Soares P., Machado Á. R. – Surface modification of medical-grade Ni55.6Ti44.4 alloy via enhanced machining characteristics of Zn powder mixed-μ-EDM. Surf. Coat. Technol., **425** (2021) 127725. https://doi.org/10.1016/j.surfcoat.2021.127725.
36. Mwangi J. W., Bui V. D., Thüsing K., Hahn S., Wagner M. F. X., Schubert A. – Characterization of the arcing phenomenon in micro-EDM and its effect on key mechanical properties of medical-grade Nitinol. J. Mater. Process. Technol., **275** (2020) 116334. https://doi.org/10.1016/j.jmatprotec.2019.116334.